Efficient computation of the dispersion interaction with density-functional theory

Jing Kong,[1,*] Zhengting Gan,[1] Emil Proynov,[1] Marek Freindorf,[2] and Thomas R. Furlani[2]
[1]*Q-Chem, Inc., 5001 Baum Boulevard, Pittsburgh, Pennsylvania 15213, USA*
[2]*Center for Computational Research, University at Buffalo, State University of New York, 701 Ellicott Street, Buffalo, New York 14203, USA*

(Received 31 July 2008; published 30 April 2009)

One of the major deficiencies of the standard density functionals is their inability to describe dispersion interactions. Becke and Johnson recently proposed a conceptually simple yet accurate dispersion model called the exchange-dipole moment (XDM) model, which allows the calculation of both intermolecular and intramolecular dispersion interactions with density functional theory (DFT). In this paper, we present an efficient self-consistent-field (SCF) solution of the XDM model. We also give detailed analysis of the post-SCF approach in which the dispersion term is added to the Hamiltonian as a perturbation, and show that it has an error on the order of 10^{-5} in density matrix due to the addition of dispersion to the Hamiltonian. In addition, for gradient calculations with respect to the atomic movement, we introduce a further approximation in which the electronic part of the XDM gradient formula is omitted, and show that it yields an error smaller than 10^{-3} a.u. These approximations offer a simple and efficient route with good precision for the implementation of XDM model and other dispersion models into existing DFT codes. The effectiveness of our implementation is demonstrated through several examples. The first example shows that inclusion of the XDM model leads to much more accurate prediction of enthalpies of formation of straight-chain alkanes than does the Becke three-parameter Lee-Yang-Parr (B3LYP) functional. The inclusion of the dispersion is also shown to improve the accuracy in the calculation of isomerization energies and bond-dissociation energies of alkanes. The last example shows that the qualitative difference in optimal geometries of a tyrosine-glycine peptide, calculated using the B3LYP functional and the second-order Møller-Plesset method, essentially disappears when XDM is added to the DFT calculation.

DOI: 10.1103/PhysRevA.79.042510 PACS number(s): 31.15.eg, 31.15.es, 31.15.xr

I. INTRODUCTION

Density-functional theory (DFT) has been the method of choice for computational chemistry for more than a decade, especially for molecular systems with more than a few dozen atoms, because it is accurate and computationally efficient. While standard DFT functionals describe chemical bonds well, one major deficiency is their inability to describe dispersion interactions [van der Waals (vdW) interactions] that exist between any two well-separated atoms. Although relatively weak compared to normal chemical bonds, dispersion interactions nonetheless play a crucial role in a wide range of fields, including structural biology (DNA, proteins, etc), surface chemistry, and polymer science. The deficiency of DFT with respect to accurately modeling dispersion interactions is well known, and, not surprisingly, efforts have been made to address this problem. One approach is to include vdW complexes (dimers that are bound by dispersion) in the training sets when the empirical parameters of the functionals are optimized. It is based on the observation that some exchange functionals predict an attractive potential-energy curve in the region where density is small and the density gradient is large [1]. An example of such a functional is M06 [2]. However, this type of functional does not yield the correct long-range R^{-6} behavior. Another approach is to explicitly add the dispersion interaction between two well-separated electron densities based on physical arguments [3–7]. While these methods display the correct asymptotic behavior, they have not been shown to be applicable for intramolecular interactions or to be efficient. For instance, Dion *et al.* [8] proposed a simplified version of an earlier model [4], which was implemented self-consistently as a density-functional model [9,10]. It is however computationally demanding, involving double numerical integrations. The current practical solution to the DFT dispersion problem is to add an empirical dispersion term based on an analogy to the vdW term in molecular mechanics [11–16]. While this method is simple to implement and adds little computational cost, its accuracy is ultimately limited by the fact that it does not take into account the variation in the electronic structure of an atom in a molecular system.

Recently Becke and Johnson (BJ) [17–21] published a new model for the dispersion interaction, called exchange-dipole moment (XDM) model. The XDM model stipulates that the dispersion attraction between two molecules is due to the dipole moment of the instant exchange hole of one molecule and the induced dipole moment of the second molecule. This model is conceptually simple and yet has been shown to yield very accurate dispersion coefficients (the coefficients to R^{-6}, R^{-8}, and R^{-10}) without empirical fitting parameters Furthermore, it can be applied to both intermolecular and intramolecular interactions with a simple density-partitioning scheme and a damping formula with one or two fitting parameters. To quantum-chemical practitioners, the XDM model is especially appealing because it can be made to depend only on the electron spin densities and their gradients, which are the same list of variables as most of the

*Corresponding author; jkong@q-chem.com

current functionals, making it possible to utilize existing efficient numerical algorithms [22,23].

We have recently devised an efficient implementation of the XDM model for energy and nuclear derivatives in the Q-CHEM program [24], which enables structural and vibrational calculations with vdW interactions to be carried out with little additional computational cost. The full self-consistent-field (SCF) calculation of the DFT energy and calculation of the full analytical gradient allow routine DFT calculations with electronic dispersion effect. Furthermore, we will demonstrate the effectiveness of a post-SCF implementation that treats the dispersion interaction as a perturbation while still obtaining the energy and nuclear derivatives with sufficient accuracy. In addition, we will show that negligible error is introduced by excluding the electronic part of the dispersion from the nuclear derivative calculation. This has important practical implications because the dispersion interaction has complicated dependency rules on the electron spin densities and their gradients, making its efficient implementation difficult, or even impractical.

The effectiveness of our implementation of the XDM model will be illustrated through some exemplary cases where DFT has failed before in a remarkable way. One such case is the total energy of alkanes. It has been reported that Becke three-parameter Lee-Yang-Parr (B3LYP) functional, the most popular DFT functional, underestimates the total energy of the linear *n*-alkanes with the error increasing as the size of the alkane increases [25]. Furthermore, it has been found that B3LYP tends to underestimate the energy of the branched isomer of the alkane [26] and the dissociation energy of simple organic molecules [27]. One possible explanation offered for the observed errors was the lack of dispersion correlation. The last case considered is the structure of a dipeptide (tyrosine-glycine), where B3LYP and the second-order Møller-Plesset (MP2) method give remarkably different structures for the same conformer [28]. The MP2 results were assumed to be more reliable since these include dispersion interactions.

II. CALCULATION OF DISPERSION ENERGY WITH XDM

Fundamental to the XDM model is the calculation of the norm of the dipole moment $\mathbf{d}$ of the exchange hole at a given point $\mathbf{r}$:

$$\mathbf{d}_\sigma(\mathbf{r}) = -\int h_\sigma(\mathbf{r},\mathbf{r}')\mathbf{r}' d^3\mathbf{r}' - \mathbf{r}, \tag{1}$$

where σ is the symbol for the spin and $h_\sigma(\mathbf{r},\mathbf{r}')$ is the exchange-hole function. Two types of exchange-hole functions were employed by BJ. One was the Hartree-Fock (HF) exchange hole that depends explicitly on the occupied molecular orbitals (MOs). The other was the Becke-Roussel (BR) model exchange hole for the Becke-Roussel exchange functional (BR89) [29]. Although BJ employed the HF exchange-hole function most of the time, they pointed out that BR exchange-hole function yields essentially the same results. In our implementation, we chose the BR exchange hole because of its computational efficiency. It is a function of the (spin-resolved) electron density, its gradients, and the kinetic-energy density, i.e., the same set of variables as for meta-generalized gradient approximation functionals. Accordingly, it can be evaluated in linear scaling with respect to the size of the system. In contrast, using HF exchange-hole function requires the evaluation of MO pairs at each grid point with the numerical integration, the computational cost of which scales quadratically to cubically with respect to the size of the system.

The original BR exchange model is not given in closed analytic form and requires the solution of a nonlinear equation at each grid point. In our implementation, we have developed an analytical expression by using nonlinear interpolation and spline techniques. While the details of the analytical expression have been published elsewhere [30], it suffices to say that the fitting produces a very small mean absolute deviation on the order of 10^{-7} for the whole range of densities and practically identical atomization energies and geometries compared with the numerical solution. Furthermore, the analytical expression makes it more feasible to calculate and facilitate the derivation of derivatives necessary for precise calculations of the potential of the XDM energy functional and of the gradients with respect to nuclear motions as discussed below.

In BJ's original implementation, the dispersion energy was added to the total DFT energy as a perturbation, i.e., the electron spin densities not being optimized with respect to the total energy through the SCF method. The efficient calculation of the forces among the atoms, required for a structural computation, relies on the optimized densities [31]. However, since the dispersion energy is a small fraction of the total energy, it is quite possible that the added dispersion term would not alter the electron densities significantly once the latter are optimized with respect to the other parts of the functional. Hence, the perturbative approach may yield an excellent approximation to the precise SCF solution. In this paper, we will compare the two approaches for the calculation of the DFT energy with XDM and its gradient with respect to nuclear motions.

BJ proposed two forms for the dispersion energy. One includes interatomic R^{-6} interactions only [17–19], and the other includes higher-order terms (R^{-6}, R^{-8}, R^{-10}) [20,21]. We chose the former for the investigation of the effect of SCF because the formalism is somewhat simpler for the derivation of the corresponding Fock matrix elements. We will denote this form of XDM as XDM6 and the one including higher-order terms will be denoted as XDM10. The formula for the dispersion energy within the XDM6 framework is

$$E_{vdW} = \sum_{i>j} E_{vdW,ij} = -\sum_{i>j} \frac{C_{6,ij}}{R_{ij}^6 + \kappa C_{6,ij}/(E_i^C + E_j^C)}. \tag{2}$$

In this equation, R_{ij} is the distance between two atoms i and j, and $C_{6,ij}$'s are the interaction coefficients, the calculation of which will be shown below. The second term in the denominator is the damping factor so that the dispersion energy becomes a constant as the two atoms come close, which allows the calculation of intramolecular dispersion. In the damping term, E_i^C is the correlation energy of the free atom i,

TABLE I. Energies of vdW molecular complexes obtained with the B3LYP(XDM6) and B3LYP+XDM6 methods using 6-31G* basis set. E_1 is the dispersion energy with B3LYP(XDM6), E_2 is the total B3LYP(XDM6) energy, E_3 is the dispersion energy with B3LYP+XDM6, and E_4 is the total B3LYP+XDM6 energy. (The values of E_3 and E_4 are not directly listed.) Direct inverse of iterative space (DIIS) error measures the deviation of the density matrix compared to the SCF-converged one. All energy values are in a.u.

			$\log_{10}(\|\ \|)$				
Complex	E_1	E_2	E_4-E_2	DIIS error	E_1/E_2	$(E_4-E_2)/E_2$	$(E_3-E_1)/E_1$
He-He	−0.000034	−5.814087	−9.70	−5.30	−5.23	−10.46	−5.23
He-Ne	−0.000094	−131.801563	−8.80	−5.52	−6.15	−10.97	−4.77
He-Ar	−0.000113	−530.424174	−8.22	−5.17	−6.67	−11.26	−4.27
Ne-Ne	−0.000172	−257.789139	−8.92	−5.72	−6.18	−11.41	−5.16
CH_4HF	−0.002570	−140.943865	−7.25	−5.20	−4.74	−9.52	−4.66
H_2S-H_2S	−0.004121	−798.777403	−6.54	−4.73	−5.29	−10.01	−4.15
Ph-Ph	−0.023903	−464.519381	−5.62	−5.12	−4.29	−8.42	−4.00

and κ is a dimensionless empirical parameter. We will use $\kappa=800$ as suggested by BJ [19], which is optimized for a set of weakly bound systems with Hartree-Fock plus Becke-Roussel correlation functional [32].

Although the above expression of dispersion energy is the same as the molecular mechanics-like empirical formulas [11–15], the coefficients $C_{6,ij}$ are determined differently. In the empirical formalism, the coefficients are constants obtained by fitting to experimental and theoretical data. In the XDM model, they are functions of electron spin densities through the exchange-hole function, the atomic polarizability, and the density partition and thus take into account the changing environment of an atom in a molecule. To evaluate the dispersion in the SCF framework, one needs to evaluate its contribution to the Fock matrix by taking the derivative of E_{vdW} with respect to the spin-resolved density matrix [33]:

$$F^{\sigma}_{\mu\nu}=\frac{\partial E_{vdW}}{\partial P^{\sigma}_{\mu\nu}}=-\sum_{i\neq j}\frac{E^2_{vdW,ij}R^6_{ij}}{C^2_{6,ij}}\frac{\partial C_{6,ij}}{\partial P^{\sigma}_{\mu\nu}}. \tag{3}$$

$C_{6,ij}$ is a complicated function of electron densities ρ_σ $[\sigma=(\alpha,\beta)]$, their gradients $\nabla\rho_\sigma$, the Laplacians $\nabla^2\rho_\sigma$, and the kinetic-energy densities τ_σ. After taking the derivative $\partial C_{6,ij}/\partial P^{\sigma}_{\mu\nu}$, the final expression for the XDM contribution to the Fock matrix becomes

$$F^{\sigma}_{\mu\nu}=-\int\frac{\partial\rho_\sigma}{\partial P^{\sigma}_{\mu\nu}}\sum_i[G_iw_ir_i^3+H_iw_i(d^2_\alpha+d^2_\beta)]$$
$$-\int\sum_{\xi_\sigma}\frac{\partial d^2_\sigma}{\partial\xi_\sigma}\frac{\partial\xi_\sigma}{\partial P^{\sigma}_{\mu\nu}}\sum_i H_iw_i\rho,$$
$$\xi_\sigma=(\rho_\sigma,\nabla\rho_\sigma,\nabla^2\rho_\sigma,\tau_\sigma). \tag{4}$$

The details and the derivations of the above equations are given in Appendix A. For the efficiency of calculation, the quantities that are independent of electron positions such as G_i and H_i can be calculated with little CPU cost before the loop over the grid points. The only additional loop in evaluating the dispersion contribution to the Fock matrix remains the one over the atoms overlapping with the current grid point. The cost associated with this loop is minuscule compared to the other major steps in a DFT calculation.

It is important to note that XDM is designed to be an add-on functional and therefore can in principle be combined with other functionals. BJ used the Hartree-Fock exchange and the Becke-Roussel correlation functional as reference functionals when optimizing the damping parameters. We choose to combine XDM (with its original parameters) with B3LYP [34,35] instead, as it is the most widely used functional to date and has been proven to be versatile. We will denote the SCF solution of the combination of B3LYP and XDM6 as "B3LYP(XDM6)" and the addition of XDM6 to the SCF solution of B3LYP, i.e., the pertubative approach, as "B3LYP+XDM6."

Table I lists the results of our energy calculations with B3LYP(XDM6) and B3LYP+XDM6 for some van der Waals complexes. The basis set is 6-31G* with the integration grid of pruned 50 radial points and 194 angular points [36]. [The basis-set superposition error (BSSE) is not relevant here because only the total energies of the complexes are compared.] The second column of Table I lists the dispersion energy (E_1) of each complex. One can see that it increases with the size of the system (in either the number of atoms or the number of electrons). The third column lists the total energy as calculated with SCF (E_2). The fourth column displays the absolute differences ($\log_{10}|E_4-E_2|$) in the total energies of the two methods, with E_4 being the total energy of B3LYP+XDM6. As one can see, the error introduced by the perturbative approach is orders of magnitude smaller than the dispersion energy, and it increases with the size of the system. The same trend is observed with the dispersion energy. However, the small difference in total energy does not necessarily indicate that the difference in electron density between the two approaches is negligible. Listed in the fifth column is the so-called DIIS error which is the root mean square of the permutation of the density and the Fock matrix. DIIS error is routinely used to measure the SCF convergence. In Q-CHEM, an SCF energy calculation is considered converged when this error is smaller than 10^{-5} for a single-point calculation, and smaller than 10^{-8} for a calculation of energy gradient with respect to nuclei used in a molecular geometry optimization. The DIIS error listed in Table I is the result of using the B3LYP density matrix to build the Fock matrix with the dispersion functional added to the Hamiltonian. Thus, it measures the error of the B3LYP density matrix as an approximation to the solution of B3LYP(XDM). As one can see, the error of the B3LYP density matrix is about 10^{-5} and does not change significantly with respect to the molecular size. This trend is different from that of the dispersion energy.

To help understand these two trends with respect to the molecular size, we calculated two additional quantities that are listed in Table I. One is the fraction of the dispersion energy relative to the total DFT energy for each molecule (sixth column). The other is the absolute value of the error of the perturbative method in energy relative to the total energy (seventh column). From these quantities, it is evident that the dispersion energy relative to the total DFT energy does not vary much with respect to the size of the molecule and is similar in magnitude to that of the DIIS error. On the other hand, the relative error in energy of the perturbative method is roughly equal to the square of the dispersion energy relative to the total energy (E_1/E_2). (Note that the numbers listed in these columns are in logarithmic scale.) This can be explained as follows. The reference (B3LYP) density matrix is obtained from the diagonalization of a Hamiltonian that deviates slightly from the "true" Hamiltonian due to the lack of the dispersion term, and therefore has an error of similar magnitude to that of the deviation. The deviation in the Hamiltonian can be approximately measured by the magnitude of the dispersion energy relative to the total energy, which explains the similarity between the fifth and sixth columns. It is useful in this vein to compare the relative total energy since the density matrix is always normalized. The total energy calculated with this slightly deviated density matrix will have an error that is proportional to the square of the deviation of the density, since the energy is invariant to the first order of the SCF-converged density matrix. It should be pointed out that the range of the dispersion energy relative to the total energy ($\sim 10^{-5}$) is consistent with BJ's estimation that the dispersion energy is about 1/1000 of the correlation energy [19], and the fact that the correlation energy is about 1/100 of the total energy. For completeness we also list the error the deviated density matrix causes to the dispersion energy alone, which is roughly proportional to the errors of the density matrix. This is not surprising given that the dispersion interaction coefficients are more or less proportional to the electron density. Overall, we can conclude from Table I that the perturbative method introduces an error on the order of 10^{-5} in the density matrix, and its error in total energy is approximately equal to the square of the error in density matrix.

III. NUCLEAR DERIVATIVES OF THE DISPERSION ENERGY

The significance of the error of the perturbative scheme can also be measured by its impact on the calculation of the analytical gradient of the total DFT energy with respect to the nuclear motion. The efficient evaluation of the analytical gradient depends on the SCF convergence of the DFT energy and densities. Assuming the SCF convergence of the densities, the additional gradient due to the dispersion interaction [Eq. (2)] has two parts, classic and electronic:

$$E_{vdW}^{\mathbf{x}} = \sum_{i\neq x} \frac{6E_{vdW,xi}^2 R_{xi}^4}{C_{6,ix}} \mathbf{R}_{xi} - \sum_{i\neq j} \frac{E_{vdW,ij}^2 R_{ij}^6}{C_{6,ij}^2} C_{6,ij}^{[\mathbf{x}]}, \qquad (5)$$

where $\mathbf{x}$ is a nuclear perturbation. The first term in the above equation is the classic part, assuming the dispersion coefficients do not change with the nuclear perturbation. $C_{6,ij}^{[\mathbf{x}]}$ in the second term is the partial derivative of the dispersion coefficient due to the movement of the basis functions of the perturbing nucleus, reflecting the changing electronic environment. The final expression for the second term is given by Eq. (B6) of Appendix B, along with the derivation. It should be noted that the major computational step of evaluating this equation is the same as in a regular DFT functional; i.e., little additional computational cost is incurred by adding the XDM dispersion force.

The optimized geometries of the complexes with the full analytical gradient are listed in Table I with B3LYP(XDM6). The approximate B3LYP+XDM6 gradients based on the B3LYP densities are calculated at those geometries, and the largest error of the gradient components for each complex is listed in the second column of Table II. The errors are on the order of 10^{-5} a.u. or less, much smaller than the usual convergence criterion of a geometry optimization. This magnitude of error is perhaps not surprising since it should be proportional to the error of the density matrices.

We have also examined the approximation of including only the classical part of the XDM gradient calculation within the B3LYP+XDM. Our conjecture is that the contribution of the electronic part of this gradient may be negligible for the following two reasons. One is that the dispersion energy changes much more rapidly with respect to the interatomic distance due to its R^{-6} scaling. Second, the shape of the exchange hole, which determines the dispersion coefficient, is predominantly influenced by the local bonding structure, and will likely change little during a conformational change, in which the dispersion plays an important role. This approximation will be denoted as CG. Listed in the third column of Table II is the largest error of the gradient components for each complex with B3LYP+XDM6 with the CG approximation (denoted as B3LYP+XDM6+CG), compared to the full implementation of the analytical gradient with B3LYP(XDM6). As one can see, the largest error is 2.5×10^{-4} a.u. among the complexes [$(C_6H_6)_2$], which is within the tolerance of regular geometry optimizations.

To examine further the applicability of B3LYP+XDM6 with the CG approximation to larger systems, we have calculated the errors of the analytical gradients of this scheme with different basis sets for two floppy systems: a cluster of 10 methane molecules [$(CH_4)_{10}$] and a cluster of 20 water molecules surrounding a methane molecule [$(H_2O)_{20}CH_4$]. The structures of the two clusters are shown in Fig. 1. The structure of $(CH_4)_{10}$ is optimized with B3LYP(XDM6) with

TABLE II. Errors of the first and second nuclear derivatives of the dispersion interaction obtained using the B3LYP+XDM6 functional with and without classic gradient (CG) approximation. The errors of the second derivatives are measured by the errors in the calculated harmonic frequencies.

	Errors of first derivatives (a.u.)		Errors of harmonic frequencies (cm^{-1})
Complex	B3LYP+XDM6	B3LYP+XDM6 with CG	B3LYP+XDM6 with CG
He-He	0.0000000	0.0000000	0.0
He-Ne	0.0000000	0.0000001	0.0
Ne-Ne	0.0000001	0.0000007	0.0
Ne-Ar	0.0000000	0.0000003	0.0
H_2S-H_2S	0.0000187	0.0000245	1.7
CH_4-NH_3	0.0000175	0.0000259	4.0
CH_4-HF	0.0000121	0.0000228	2.8
Ph-Ph	0.0000371	0.0002509	2.0

6-311++G(d,p) and full analytical gradient. The maximum component of the nuclear gradients is 1.7×10^{-4} a.u. at the converged geometry. The nuclear gradient of the same geometry is calculated with B3LYP+XDM6+CG, with a resulting maximum component of 1.8×10^{-4} a.u. The same calculations are carried out for $(H_2O)_{20}CH_4$ with a 6-31+G(d) basis set. The gradient calculated with B3LYP+XDM6 +CG has here a maximum component of 5.7×10^{-4} a.u., compared with that of full analytical gradient, 2.7×10^{-4} a.u. Overall, the error of CG approximation is on the order of less than 10^{-3} a.u. when combined with the post-SCF approximation.

The CG approximation for the calculation of the gradient simplifies the implementation of the analytical gradient formula, and even more so for the second derivative of the DFT energy, as the algorithm for the second derivative is considerably more complicated. The fourth column of Table II lists the largest errors in harmonic frequency, which are directly calculated from the second nuclear derivatives, using the B3LYP+XDM and the CG approximations for all the derivative calculations for each complex. The precise reference values are calculated with finite difference of the B3LYP(XDM6) gradients. As one can see, the largest difference is about 4 cm^{-1}, which happens at a low frequency of 33 cm^{-1}, and is well within the error of a DFT harmonic frequency calculation.

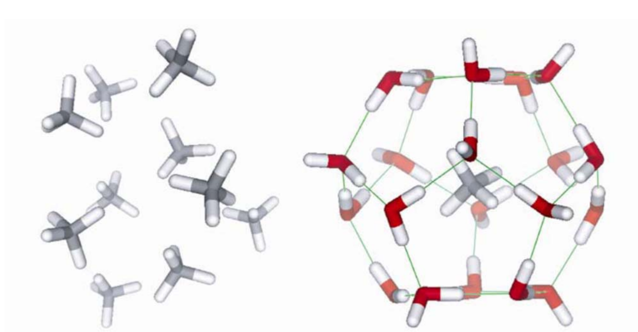

FIG. 1. (Color online) Optimized structures of the methane cluster and the water-methane clusters.

We note that while the error of the perturbative scheme has been illustrated only for the XDM6 model, the underlying argument should be general for the reason that the dispersion is very small compared to the total energy. Therefore it should be a good approximation to the XDM10 model that includes higher-order terms, and for other electronic dispersion models. Indeed, Thonhauser *et al.* [9] showed qualitatively through some exemplary calculations within the dispersion model of Dion *et al.* [8] that the perturbative and the SCF approaches yield approximately the same results. This is noteworthy as the derivative of the XDM10 with respect to the electron density, as well as those of other models, is very complicated.

IV. APPLICATIONS OF THE XDM MODEL

With the efficient implementation of the XDM model for derivatives presented here, it is now possible to routinely carry out DFT calculations with dispersion effects included. We will demonstrate the effectiveness of this methodology by applying it to some well-studied cases in the literature, most of which require calculations of nuclear gradients of the intermolecular and intramolecular dispersion energies. The grid for the numerical integration of the exchange-correlation (XC) functionals is composed of unpruned 120 radial points (Euler-Maclaurin scheme [37]) and 302 angular points (Lebedev scheme [38]).

A. Total energies of linear alkanes

In their comparison study of Gaussian-3 theory [39] versus DFT, Redfern *et al.* [25] calculated the enthalpies of formation of the *n*-alkanes with B3LYP and observed that there is a significant accumulation of errors as the chain length increases, with an error as large as 30 kcal/mol for hexadecane. Dispersion was suspected as one possible source of error. We recalculated the enthalpies of formation for the same series of molecules using the same basis set [6-311 +G(3df,2p)] and structures but with B3LYP+XDM6 and B3LYP+XDM10 functionals. The results are listed in Fig. 2

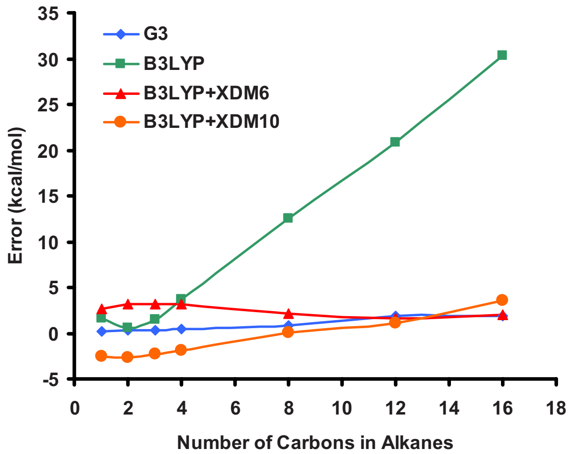

FIG. 2. (Color online) Plots of deviations from experimental formation enthalpies of straight-chain alkanes obtained at G3, B3LYP, B3LYP+XDM6, and B3LYP+XDM10 levels of theory.

and Table III. As one can see, both versions of XDM have essentially corrected the erratic behavior of B3LYP total energy with respect to the size of the system. In particular, the error for hexadecane is dramatically reduced from 30 to 3–4 kcal/mol. It also shows the generality of the XDM model as the few adjustable parameters of the model were not reoptimized with B3LYP. XDM10 still shows a slight increase in error with respect to the molecular size, but it is greatly reduced from the error of B3LYP. The residual error could in part be due to the fact that the damping function for XDM10 is optimized specifically for B97 functional. We intend to investigate this in more detail in a subsequent study.

B. Isomerization energy of octane

After the finding that standard B3LYP fails to predict the total energy of linear alkanes, various studies on different alkane isomers have shown that DFT often fails to accurately predict the isomerization energy as well. The lack of dispersion in the functionals has been attributed to the problem [26,40,41]. In particular, it has been found [26] that B3LYP favors the linear octane (C_8H_{18}) versus its branched isomer by 8.4 kcal/mol (the structures of linear and the branched octanes are shown in Fig. 3). This is in sharp disagreement with the experimental result, which favors the branched isomer by about 1.9 kcal/mol. MP2, on the other hand, favors the branched isomer by 4.6 kcal/mol. We have calculated these two octane conformers using a similar approach, namely, the full geometry optimization calculations using the MP2/TZV(d,p) method (TZV denotes triple zeta valence), followed by a single-point energy calculation using the B3LYP+XDM6 and the B3LYP+XDM10 methods with the augmented correlation-consistent polarized valence quadruple zeta (aug-cc-pVQZ) basis set. Our results show that the linear octane is predicted to be more stable than the branched octane by 4.0 kcal/mol with B3LYP+XDM6 method and by 5.2 kcal/mol with B3LYP+XDM10. These estimates are an improvement compared to those of B3LYP and in the same range as those by the empirical vdW method (5.5 kcal/mol) [26]. However, they still fail to predict the correct relative stability. The remaining errors after the dispersion correction support the observation in Ref. [26] that the dispersion interaction is not the only major effect that is missing from the current functionals.

TABLE III. Deviations in kcal/mol from experimental formation enthalpies of straight-chain alkanes obtained using the B3LYP, B3LYP+XDM6, and B3LYP+XDM10 functionals.

No. of carbons in alkanes	G3	B3LYP	B3LYP+XDM6	B3LYP+XDM10
1	0.25	1.62	2.60401	−2.48108
2	0.31	0.60	3.18832	−2.72485
3	0.33	1.46	3.18150	−2.33299
4	0.40	3.69	3.12870	−1.91265
8	0.88	12.50	2.10234	0.01937
12	1.88	20.90	1.59216	1.13049
16	1.91	30.26	2.06271	3.51179

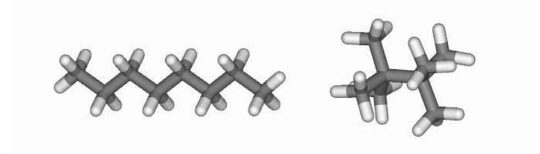

FIG. 3. The structures of the linear and the branched conformers of octane.

C. Bond-dissociation energy

Alkanes and other simple organic molecules have also been used to illustrate another deficiency of DFT, namely, the underestimation of the bond-separation energy [27,42,43]. When a molecule is dissociated into two species, the dispersion attraction between the two species inside the single molecule will disappear as they are separated after the dissociation. DFT underestimates the separation energy by not including this dispersion interaction in the energy balance. For example, Check and Gilbert [27] showed that B3LYP systematically underestimates the dissociation energies of the C-C bond of a series of progressively methyl-substituted alkanes, while MP2 overestimates it. Their results are listed in Table IV. We have calculated the dissociation energies with the B3LYP+XDM6 and B3LYP+XDM10 methods, and using the 6-311++G(d,p) basis set including a zero-point energy correction obtained from B3LYP/6-311++G(d,p). Overall, this is a very similar approach to the one used in the Ref. [27]. The results of our calculations are listed in the last two columns of Table IV. As one can see, both the XDM6 and XDM10 corrections reduced the errors. As in the case of the isomerization of octane, the remaining errors are likely due to other deficiencies of B3LYP.

D. Structure of a dipeptide

The final test case is a conformational study of a dipeptide. Van Mourik *et al.* [28] carried out high-level electronic

TABLE IV. Experimental and calculated bond-dissociation energies of the internal C-C bond (kcal/mol).

Reaction	Expt.	B3LYP	MP2	B3LYP+XDM6	B3LYP+XDM10
$(CH_3)_3C\text{-}CH_3 \rightarrow (CH_3)_3C+CH_3$	86.9	73.7	88.2	77.0	76.1
$(CH_3)_3C\text{-}CH_2CH_3 \rightarrow (CH_3)_3C+CH_2CH_3$	84.5	69.2	87.9	73.1	72.0
$(CH_3)_3C\text{-}CH(CH_3)_2 \rightarrow (CH_3)_3C+CH(CH_3)_2$	81.5	63.2	86.3	68.3	66.9
$(CH_3)_3C\text{-}C(CH_3)_3 \rightarrow (CH_3)_3C+C(CH_3)_3$	77.1	56.0	84.1	62.5	60.7

[a]Experimental data from Ref. [44].
[b]Calculations from Ref. [27].
[c]Our calculations.

structure calculations of molecular conformations and relative stabilities of tyrosine-glycine and found that the gas phase structure of the dipeptide varies qualitatively between B3LYP and MP2 optimizations. Particularly interesting is one conformation where B3LYP with 6-31+G(d) basis set yields a partially open-book structure [Fig. 4(a)], whereas MP2 predicts a closed-book structure [Fig. 4(b)] with the same basis set. Single-point calculations on those two geometries show that MP2 favors the closed-book structure by 3.1 kcal/mol and B3LYP favors the partially open-book one by 7.9 kcal/mol. The authors of the paper investigated the basis-set effect, including basis-set superposition error, and attributed the difference partially to the dispersion which is missing in the B3LYP calculation. We carried out geometry optimizations using the B3LYP+XDM6+CG and B3LYP+XDM10+CG models with the 6-31+G(d) basis set and with the CG approximation. The structure calculated by the B3LYP+XDM6 method is depicted in Fig. 4(c) (B3LYP+XDM10 predicts a very similar final geometry). As one can see, the XDM-corrected structures closely resemble the MP2 optimized closed-book structure. We have also calculated the total DFT energies of B3LYP+XDM6 and B3LYP+XDM10 at partially open-book B3LYP structure [Fig. 4(a)] and compared them with those of the respective optimized structures. B3LYP+XDM6 predicts an energy difference of 1.1 kcal/mol, and B3LYP+XDM10 predicts 1.0 kcal/mol in favor of the closed-book structures. These energy differences are smaller than that of MP2 but have the same sign. To verify the CG approximation, we also performed a geometry optimization using the B3LYP(XDM6) with full analytical gradient, which yielded a structure that was practically identical to that of B3LYP+XDM6+CG.

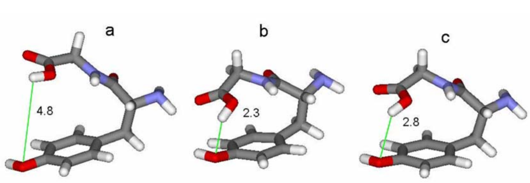

FIG. 4. (Color online) Structures of the optimal geometries of the tyrosine-glycine peptide calculated using the 6-31+G* basis set. The calculations are based on (a) B3LYP, (b) MP2, and (c) B3LYP+XDM6. The numbers indicate the distance between oxygen of tyrosine and hydrogen of glycine, measured in angstroms.

V. CONCLUSION

We have implemented a computationally efficient version of the XDM model of Becke and Johnson [17–21] for DFT calculations, which allows structural studies of both intermolecular and intramolecular electronic dispersion effects. These effects have been missing in routine DFT calculations. For the calculation of energy, we examined two approaches, a conventional SCF and a perturbative one where the electron density matrices are not reoptimized after the dispersion terms are added. We have shown that the deviation of density matrix due to the addition of dispersion is on the order of 10^{-5}, and the relative error in total energy is the square of the error in density matrix. This error in density matrix also causes an error in the nuclear gradient calculation of the same magnitude. Thus, the perturbative approach constitutes a good approximation. This finding will greatly simplify the implementation of electronic dispersion models when this level of error is acceptable. The reason is that it is far from trivial to take the derivative of the dispersion energy with respect to the density due to the complexity of the formalism. We have also examined the approximation of obtaining the nuclear derivatives with the classic part of XDM only (i.e., assuming the derivative of the dispersion coefficients is very small with respect to the nuclear motion), and found that the error is small (less than 10^{-3} a.u.) for the first and second derivatives. The new implementation was then applied to several test cases for which a lack of dispersion was suspected to be the cause of observed errors in computed energies and structures. In the case of *n*-alkane series, XDM has essentially corrected the erratic behavior of B3LYP where the error of the total energy increases with the size of the system. For the structural calculation of a dipeptide (tyrosine-glycine), the addition of the dispersion interaction with XDM has reversed a previous structure prediction with B3LYP, bringing qualitative agreement between DFT and MP2. The inclusion of dispersion with XDM has also reduced the errors of B3LYP for the isomerization energy and bond-dissociation energy of alkanes. The significant improvement of the results presented here illustrates the general applicability of the XDM model. Further improvement can be achieved by reoptimizing the parameters of the XDM model in combination with B3LYP and other accurate functionals [30,45].

ACKNOWLEDGMENTS

The work was supported by National Institutes of Health with Grants No. GM073408 and No. GM084555. J.K. would like to thank Dr. Y. Shao for technical assistance and Professor K. Jordan for helpful discussions.

APPENDIX A: THE XDM DISPERSION CONTRIBUTION TO THE FOCK MATRIX

In this appendix, we will derive the expression of the dispersion contribution to the Fock matrix based on the density-functional R^{-6}-only model [19], an early version of XDM model. In this model, the dispersion coefficients have the following expression:

$$C_{6,ij} = \frac{\alpha_i \alpha_j \langle M^2\rangle_i \langle M^2\rangle_j}{\alpha_i \langle M^2\rangle_j + \alpha_j \langle M^2\rangle_i}. \quad \text{(A1)}$$

Here α_i is the polarizability for atom i, and $\langle M^2\rangle_i$ is the average of the square of the norm of the dipole moment of the exchange hole of a point in atom i. In a molecular environment, α_i and $\langle M^2\rangle_i$ are effective atomic quantities that depend on the molecular electron density. Specifically, the electron density $\rho(\mathbf{r})$, which is the sum of the spin densities $\rho_\alpha(\mathbf{r})$ and $\rho_\beta(\mathbf{r})$, is partitioned into atomic contributions through the following weighting function $w_i(\mathbf{r})$:

$$w_i(\mathbf{r}) = \frac{\rho_i^{\text{free}}(\mathbf{r})}{\sum_j \rho_j^{\text{free}}(\mathbf{r})}, \quad \text{(A2)}$$

where $\rho_i^{\text{free}}(\mathbf{r})$ is the electron density of the free atom. With this weight function, the density of an atom in a molecule can then be defined as

$$\rho_i(\mathbf{r}) = w_i(\mathbf{r})\rho(\mathbf{r}). \quad \text{(A3)}$$

Since the polarizability of a free atom is found proportional to the volume, an effective atomic volume is defined as

$$V_i = \int \rho_i(\mathbf{r}) r_i^3 d^3\mathbf{r}, \quad \text{(A4)}$$

so that the effective atomic polarizability α_i can be defined as

$$\alpha_i = \frac{V_i}{V_i^{\text{free}}}\alpha_i^{\text{free}}. \quad \text{(A5)}$$

The other quantity that determines the C_6 value, $\langle M^2\rangle_i$, is an average over the magnitude of the dipole moment of all the exchange holes in the atom,

$$\langle M^2\rangle_i = \int \rho_i(\mathbf{r})[d_\alpha^2(\mathbf{r}) + d_\beta^2(\mathbf{r})]d^3\mathbf{r}, \quad \text{(A6)}$$

where $d_\sigma(\mathbf{r})$ is the norm of the dipole moment $\mathbf{d}_\sigma(\mathbf{r})$ of the exchange hole of the spin σ at the point $\mathbf{r}$. The norm of the BR exchange hole is simply the variable b as defined by Eq. (17) of Ref. [29]. The original solution of the BR exchange hole in Ref. [29] was numerical. We have developed an analytical fit of it [30] such that d_σ becomes an analytical function of ρ_σ, $\nabla\rho_\sigma$, $\nabla^2\rho_\sigma$, and τ_σ:

$$d_\sigma \equiv d_\sigma(\rho_\sigma, \nabla\rho_\sigma, \nabla^2\rho_\sigma, \tau_\sigma) \equiv d_\sigma(\xi_\sigma), \quad \text{(A7)}$$

$$\xi_\sigma = (\rho_\sigma, \nabla\rho_\sigma, \nabla^2\rho_\sigma, \tau_\sigma).$$

The details of the expression can be readily obtained from Ref. [30].

With $C_{6,ij}$ defined, one can now evaluate its derivative with respect to the density matrix, starting from Eq. (2):

$$F_{\mu\nu}^\sigma = -\sum_{i\neq j} \frac{E_{vdW,ij}^2 R_{ij}^6}{(\alpha_i \langle M^2\rangle_j)^2}\left(\langle M^2\rangle_j \frac{\partial \alpha_i}{\partial P_{\mu\nu}^\sigma} + \alpha_i \frac{\partial\langle M^2\rangle_j}{\partial P_{\mu\nu}^\sigma}\right). \quad \text{(A8)}$$

One can use Eqs. (A5) and (A4) to obtain the following expression for $\partial\alpha_i/\partial P_{\mu\nu}^\sigma$:

$$\frac{\partial \alpha_i}{\partial P_{\mu\nu}^\sigma} = \frac{\alpha_i^{\text{free}}}{V_i^{\text{free}}}\int w_i r_i^3 \frac{\partial \rho_\sigma}{\partial P_{\mu\nu}^\sigma}. \quad \text{(A9)}$$

(Note that the symbols $\mathbf{r}$ and $d^3\mathbf{r}$ are dropped from the above equation and the ones below for a shortened look of equations.)

Similarly, one can obtain the expression for $\partial\langle M^2\rangle_j/\partial P_{\mu\nu}^\sigma$ using Eq. (A6):

$$\frac{\partial\langle M^2\rangle_j}{\partial P_{\mu\nu}^\sigma} = \int\left(w_j(d_\alpha^2 + d_\beta^2)\frac{\partial\rho_\sigma}{\partial P_{\mu\nu}^\sigma} + w_j\rho\frac{\partial d_\alpha^2}{\partial P_{\mu\nu}^\sigma}\right). \quad \text{(A10)}$$

From Eq. (A7), we can formally obtain the expression for $\partial d_\alpha^2/\partial P_{\mu\nu}^\sigma$:

$$\frac{\partial d_\sigma^2}{\partial P_{\mu\nu}^\sigma} = \sum_\xi \frac{\partial d_\sigma^2}{\partial \xi}\frac{\partial \xi}{\partial P_{\mu\nu}^\sigma}. \quad \text{(A11)}$$

Bringing all the above expressions to Eq. (A8) yields

$$F_{\mu\nu}^\sigma = -\sum_{i\neq j}\frac{E_{vdW,ij}^2 R_{ij}^6}{(\alpha_i\langle M^2\rangle_j)^2}\Bigg[\langle M^2\rangle_j \frac{\alpha_i^{\text{free}}}{V_i^{\text{free}}}\int w_i r_i^3 \frac{\partial\rho_\sigma}{\partial P_{\mu\nu}^\sigma} + \alpha_i\int\left(w_j(d_\alpha^2+d_\beta^2)\frac{\partial\rho_\sigma}{\partial P_{\mu\nu}^\sigma} + w_j\rho\sum_{\xi_\sigma}\frac{\partial d_\sigma^2}{\partial\xi_\sigma}\frac{\partial\xi_\sigma}{\partial P_{\mu\nu}^\sigma}\right)\Bigg]. \quad \text{(A12)}$$

After some reorganization of indexes for better computational efficiency, one obtains the final expression Eq. (3) with

$$G_i = \frac{\alpha_i^{\text{free}}}{V_i^{\text{free}}}\sum_{j\neq i} A_{ij}\langle M^2\rangle_j, \quad H_i = \sum_{j\neq i} A_{ji}\alpha_j, \quad A_{ij} = \frac{E_{vdW,ij}^2 R_{ij}^6}{(\alpha_i\langle M^2\rangle_j)^2}. \quad \text{(A13)}$$

The final expression may look more complicated than a standard DFT calculation, but it has a similar cost. A standard DFT functional has in general the same variables as d_σ (although not all the variables are in every functional), and its contribution to the Fock matrix can be expressed as

$$F_{\mu\nu}^\sigma = \int \sum_\xi \frac{\partial f}{\partial \xi}\frac{\partial \xi}{\partial P_{\mu\nu}^\sigma}. \quad \text{(A14)}$$

The most CPU-intensive steps in the implementation of Eq. (A14) are the computation of the variables and the formation of the Fock matrices on the grid as they involve loops over the basis function pairs for each grid point. The evaluation of $\partial f/\partial\xi$ takes little time. In comparison, Eq. (3) adds a loop of atoms for each grid point for the calculation of XDM, the cost of which is still relatively small because the number of atoms that have effectively nonzero contribution to a grid point is much less than the number of effective basis function pairs. Furthermore, the calculation of the terms (G_i and H_i) involving double loops over the atoms can be carried out independently of the loop over the grid points. In practice, we see little CPU time increase when the XDM contribution is added to a functional that has the same variables.

APPENDIX B: THE NUCLEAR FORCE OF THE ELECTRONIC PART OF THE XDM DISPERSION

The second term in Eq. (5) can be reorganized as the following using G_i and H_i defined in Eq. (A13):

$$\sum_{i\neq j}\frac{E_{vdW,ij}^2 R_{ij}^6}{C_{6,ij}^2}C_{6,ij}^{[\mathbf{x}]}=\sum_i (G_i V_i^{\mathbf{x}}+H_i\langle M^2\rangle_i^{\mathbf{x}}). \tag{B1}$$

$V_i^{\mathbf{x}}$ in the above equation can be derived from Eqs. (A3)–(A5):

$$V_i^{\mathbf{x}}=\int (w_i^{\mathbf{x}} r_i^3\rho + w_i r_i^3\rho^{\mathbf{x}} - 3w_x r_x \mathbf{r}_x\rho\delta_{xi}) + \int^{\mathbf{x}} w_i r_i^3\rho, \tag{B2}$$

with

$$w_i^{\mathbf{x}}=(\delta_{xi}-w_i)\frac{\rho_x^{\mathrm{free},\mathbf{x}}}{\sum_j \rho_j^{\mathrm{free}}(\mathbf{r})},\quad \rho_x^{\mathrm{free},\mathbf{x}}=\sum_{\mu\nu}P_{\mu\nu}^{\mathrm{free}}(\phi_\mu\phi_\nu)^{\mathbf{x}}\delta_{\mu x}\delta_{\nu x}, \tag{B3}$$

where $P_{\mu\nu}^{\mathrm{free}}$ is the total electron density of the free atom. Of the quantities to be calculated, the gradient of the basis functions and the gradient of the total density are already available in a standard DFT gradient calculation. Here the symbol $\int^{\mathbf{x}}$ denotes taking the derivative of the weights used in the numerical integration with respect to $\mathbf{x}$:

$$\int^{\mathbf{x}} f(\mathbf{r})d^3\mathbf{r}\equiv\sum_k W_k^{\mathbf{x}}(\mathbf{r}_k)f(\mathbf{r}_k). \tag{B4}$$

The algorithm used to calculate the weight derivatives can be found in the literature [46].

Similarly, the formula for the calculation of $\langle M^2\rangle_j^{\mathbf{x}}$ can be obtained by taking the derivative of Eqs. (A6) and (A3):

$$\langle M^2\rangle_i^{\mathbf{x}}=\int\left((w_i^{\mathbf{x}}\rho+w_i\rho^{\mathbf{x}})(d_\alpha^2+d_\beta^2)+w_i\rho\sum_\xi\frac{\partial(d_\alpha^2+d_\beta^2)}{\partial\xi}\xi^{\mathbf{x}}\right) + \int^{\mathbf{x}} w_i\rho(d_\alpha^2+d_\beta^2). \tag{B5}$$

To take the advantage of the existing efficient algorithm and code for standard DFT calculations and achieve efficiency, the second term in the gradient of the dispersion energy [Eq. (B1)] can be reorganized as follows using the expressions for $V_i^{\mathbf{x}}$ and $\langle M^2\rangle_j^{\mathbf{x}}$:

$$\sum_i (G_i V_i^{\mathbf{x}}+H_i\langle M^2\rangle_i^{\mathbf{x}})=\int\left(M\rho^{\mathbf{x}}+N\rho\sum_\xi\frac{\partial(d_\alpha^2+d_\beta^2)}{\partial\xi}\xi^{\mathbf{x}}\right)+\int^{\mathbf{x}} M\rho+\int\rho[3G_x w_x r_x\mathbf{r}_x+Q(\mathbf{x})], \tag{B6}$$

with

$$L_i=G_i r_i^3+H_i(d_\alpha^2+d_\beta^2), \tag{B7}$$

$$M=\sum_i w_i L_i,\quad N=\sum_i H_i w_i,\quad Q(\mathbf{x})=\sum_i w_i^{\mathbf{x}} L_i.$$

This can be compared with the gradient of XC energy with regular DFT functionals by taking the derivative of a normal functional with respect to $\mathbf{x}$:

$$E_{XC}^{\mathbf{x}}=\int\sum_\xi\frac{\partial f}{\partial\xi}\xi^{\mathbf{x}}+\int^{\mathbf{x}} f. \tag{B8}$$

One can see that the first two terms in Eq. (B6) are similar to those in Eq. (B8) since the density is part of the ξ variables. Thus, the code for the latter can be utilized for the former. Among the various quantities to be computed in the two equations, the calculation of the variables ξ and their explicit derivatives $\xi^{\mathbf{x}}$ dominates the CPU time as they require the loop over basis function pairs for each grid point. The additional cost for the dispersion is in the calculation of the last term in Eq. (B6) and the variables in Eq. (B7). All those quantities except $Q(\mathbf{x})$ involve looping over atoms for each grid point. As discussed in Sec. II, the computational cost associated with this kind of loops takes relatively little time since only the atoms that overlap with the grid point need to be included. The calculation of $Q(\mathbf{x})$, on the other hand, involves looping over pairs of atoms that overlap with the grid point. Still, the number of such pairs is much smaller than the number of basis function pairs ($<1\%$), and thus the additional computational cost is inconsequential.

[1] Y. Zhang, W. Pan, and W. Yang, J. Chem. Phys. **107**, 7921 (1997).

[2] Y. Zhao, N. E. Schultz, and D. G. Truhlar, J. Chem. Theory Comput. **2**, 364 (2006).

[3] K. Rapcewicz and N. W. Ashcroft, Phys. Rev. B **44**, 4032 (1991).

[4] Y. Andersson, D. C. Langreth, and B. I. Lundqvist, Phys. Rev. Lett. **76**, 102 (1996).

[5] J. F. Dobson, Int. J. Quantum Chem. **69**, 615 (1998).

[6] T. Sato, T. Tsuneda, and K. Hirao, J. Chem. Phys. **126**, 234114 (2007).

[7] W. Kohn, Y. Meir, and D. E. Makarov, Phys. Rev. Lett. **80**,

4153 (1998).
[8] M. Dion, H. Rydberg, E. Schröder, D. C. Langreth, and B. I. Lundqvist, Phys. Rev. Lett. **92**, 246401 (2004).
[9] T. Thonhauser, V. R. Cooper, S. Li, A. Puzder, P. Hyldgaard, and D. C. Langreth, Phys. Rev. B **76**, 125112 (2007).
[10] J. Hooper, V. R. Cooper, T. Thonhauser, N. A. Romero, F. Zerilli, and D. C. Langreth, ChemPhysChem **9**, 891 (2008).
[11] Q. Wu and W. Yang, J. Chem. Phys. **116**, 515 (2002).
[12] S. Grimme, J. Comput. Chem. **25**, 1463 (2004).
[13] P. Jurecka, I. Černý, P. Hobza, and D. R. Salahub, J. Comput. Chem. **28**, 555 (2007).
[14] P. Hobza and J. S. T. J. Reschel, J. Comput. Chem. **16**, 1315 (1995).
[15] S. Grimme, J. Comput. Chem. **27**, 1787 (2006).
[16] J.-D. Chai and Martin Head-Gordon, Phys. Chem. Chem. Phys. **10**, 6615 (2008).
[17] A. D. Becke and E. R. Johnson, J. Chem. Phys. **122**, 154104 (2005).
[18] E. R. Johnson and A. D. Becke, J. Chem. Phys. **123**, 024101 (2005).
[19] A. D. Becke and E. R. Johnson, J. Chem. Phys. **123**, 154101 (2005).
[20] A. D. Becke and E. R. Johnson, J. Chem. Phys. **124**, 014104 (2006).
[21] E. R. Johnson and A. D. Becke, J. Chem. Phys. **124**, 174104 (2006).
[22] J. Kong, S. T. Brown, and L. Fusti-Molnar, J. Chem. Phys. **124**, 094109 (2006).
[23] S. T. Brown and J. Kong, Chem. Phys. Lett. **408**, 395 (2005).
[24] Y. Shao *et al.*, Phys. Chem. Chem. Phys. **8**, 3172 (2006).
[25] P. C. Redfern, P. Zapol, L. A. Curtiss, and K. Raghavachari, J. Phys. Chem. A **104**, 5850 (2000).
[26] S. Grimme, Angew. Chem., Int. Ed. **45**, 4460 (2006).
[27] C. E. Check and T. M. Gilbert, J. Org. Chem. **70**, 9828 (2005).
[28] T. van Mourik, P. G. Karamertzanis, and S. L. Price, J. Phys. Chem. A **110**, 8 (2006).
[29] A. D. Becke and M. R. Roussel, Phys. Rev. A **39**, 3761 (1989).
[30] E. Proynov, Z. Gan, and J. Kong, Chem. Phys. Lett. **455**, 103 (2008).
[31] P. Pulay, Mol. Phys. **17**, 197 (1969).
[32] A. D. Becke, J. Chem. Phys. **88**, 1053 (1988).
[33] J. A. Pople, P. M. W. Gill, and B. G. Johnson, Chem. Phys. Lett. **199**, 557 (1992).
[34] A. D. Becke, J. Chem. Phys. **98**, 5648 (1993).
[35] P. J. Stephens, F. J. Devlin, C. F. Chabalowski, and M. J. Frisch, J. Phys. Chem. **98**, 11623 (1994).
[36] P. M. W. Gill, B. G. Johnson, and J. A. Pople, Chem. Phys. Lett. **209**, 506 (1993).
[37] C. W. Murray, N. C. Handy, and G. J. Laming, Mol. Phys. **78**, 997 (1993).
[38] V. I. Lebedev and A. L. Skorokhodov, Dokl. Math. **45**, 587 (1992).
[39] L. A. Curtiss, K. Raghvachari, P. C. Redfern, V. Rassolov, and J. A. Pople, J. Chem. Phys. **109**, 7764 (1998).
[40] P. R. Schreiner, A. A. Fokin, R. A. Pascal, Jr., and A. de Meijere, Org. Lett. **8**, 3635 (2006).
[41] M. D. Wodrich, C. Corminboeuf, and P. v. R. Schleyer, Org. Lett. **8**, 3631 (2006).
[42] T. M. Gilbert, J. Phys. Chem. A **108**, 2550 (2004).
[43] M. D. Wodrich, Clemence Corminboeuf, Peter R. Schreiner, Andrey A. Fokin, and Paul von Rague Schleyer, Org. Lett. **9**, 1851 (2007).
[44] Y.-R. Luo, *Handbook of Bond Dissociation Energies in Organic Compounds* (CRC, New York, 2003), Chap. 4.
[45] E. Proynov and J. Kong, J. Chem. Theory Comput. **3**, 746 (2007).
[46] B. G. Johnson and M. J. Fisch, J. Chem. Phys. **100**, 7429 (1994).